arXiv:2309.10164v2 [cs.RO] 21 Sep 2025

A Scalable Multi-Robot Framework for Decentralized and Asynchronous Perception-Action-Communication Loops

Saurav Agarwal*, Frederic Vatnsdal*, Romina Garcia Camargo, Vijay Kumar, and Alejandro Ribeiro

***Abstract*—Collaboration in large robot swarms to achieve a common global objective is a challenging problem in large environments due to limited sensing and communication capabilities. The robots must execute a Perception-Action-Communication (PAC) loop—they perceive their local environment, communicate with other robots, and take actions in real time. A fundamental challenge in decentralized PAC systems is to decide *what* information to communicate with the neighboring robots and *how* to take actions while utilizing the information shared by the neighbors. Recently, this has been addressed using Graph Neural Networks (GNNs) for applications such as flocking and coverage control. Although conceptually, GNN policies are fully decentralized, the evaluation and deployment of such policies have primarily remained centralized or restrictively decentralized. Furthermore, existing frameworks assume sequential execution of perception and action inference, which is very restrictive in real-world applications. This paper proposes a framework for asynchronous PAC in robot swarms, where decentralized GNNs are used to compute navigation actions and generate messages for communication. In particular, we use aggregated GNNs, which enable the exchange of hidden layer information between robots for computational efficiency and decentralized inference of actions. Furthermore, the modules in the framework are asynchronous, allowing robots to perform sensing, extracting information, communication, action inference, and control execution at different frequencies. We demonstrate the effectiveness of GNNs executed in the proposed framework in navigating large robot swarms for collaborative coverage of large environments.**

***Index Terms*—Graph Neural Networks, Decentralized Control, Multi-Robot Systems, Robot Swarms**

I. Introduction

Decentralized collaboration for navigation of robot swarms through an environment requires high-fidelity algorithms that can efficiently and reliably handle Perception-Action-Communication (PAC) in a feedback loop (Figure 1). The primary challenge in such systems is to decide *what* a robot should communicate to its neighbors and *how* to use the communicated information to take appropriate actions. Graph Neural Networks (GNNs) [1] are particularly suitable for this task as they can operate on a communication graph and can learn to aggregate information from neighboring robots to take decisions [2], [3]. They have been shown to be an effective learning-based approach for several multi-robot applications, such as flocking [2], [4], coverage control [5], path planning [6], and target tracking [7]. Furthermore, GNNs exhibit several desirable properties for decentralized systems [8]: (1) *transferability* to new graph topologies not seen in the training set, (2) *scalability* to large teams of robots, and (3) *stability* to graph deformations due to positioning errors.

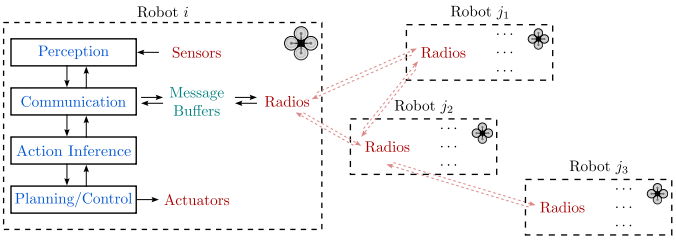

Fig. 1. Perception-Action-Communication (PAC) in robots: The perception module utilizes the sensor data to perform tasks such as SLAM, semantic mapping, and object detection. The communication module is responsible for the exchange of information between robots via message buffers, thereby enabling the coordination and collaboration of robots. Limited communication capabilities restrict robots to exchanging messages only with neighboring robots. The planning and control module takes actions from the action module, plans a trajectory, and sends control commands to the actuators. In this paper, we use Graph Neural Networks (GNNs) to compute the messages to be exchanged, the aggregation of received messages, and action inferencing.

Neural networks on graphs have been developed in the past decade for a variety of applications such as citation networks [1], classification of protein structures [9], and predicting power outages [10]. A fundamental difference between these applications and the collaboration of robot swarms is that the graph is generally static, whereas the robots are continuously moving, resulting in a dynamic and sparse communication graph. Moreover, control policies are executed on robots in real-time with limited computational capabilities, which makes it imperative to provide an efficient framework for decentralized inference.

Some of these challenges have been addressed in recent works on GNNs for multi-robot systems. Tolstaya *et al.* [2] proposed an aggregated GNN model that uses aggregated features with hidden outputs of the internal network layers for decentralized GNNs. Gama *et al.* [4] proposed a framework for learning GNN models using imitation learning for decentralized controllers. Despite these recent advances and the conceptually decentralized nature of GNNs, evaluation and deployment of GNN policies have largely remained centralized or assume fully connected communication graphs [5], [11]. A primary reason for this is that training of GNNs is usually performed in a centralized setting for efficiency, and there is a lack of asynchronous PAC frameworks for evaluation and deployment of these policies in decentralized settings.

Recently, Blumenkamp *et al.* [12] proposed a framework

*These authors contributed equally.

The authors are affiliated with the University of Pennsylvania, USA. {sauravag,vatnsdal,rominag,kumar,aribeiro}@upenn.edu.
This work was supported by grants ARL DCIST CRA W911NF-17-2-0181 and ONR N00014-20-1-2822.

for running decentralized GNN-based policies on multi-robot systems, along with a taxonomy of network configurations. While our framework focuses more on the architecture design for PAC systems and less on networking protocols, a key difference is that we enable the asynchronous execution of different modules in the framework. In real-world applications with robots running PAC loops, a robot may need to perform perception tasks such as sensing, post-processing of sensor data, constructing semantic maps, and SLAM, which results in a computationally expensive perception module. Most prior work on GNNs for multi-robot systems [2], [4] do not consider the entire PAC loop and focus on action inference. This results in a sequential computation—first, the system evolves, providing a new state, and then the GNN module is executed to generate the message and action, and the process is repeated. In robotics, it is desirable to perform computations asynchronously, which is generally already done for low-level sensing, communication, and control. This motivates the need for a fully asynchronous PAC framework, where the GNN module can be executed at a higher frequency than the perception module. An asynchronous GNN module enables multiple rounds of GNN message aggregation, thereby diffusing information over a larger portion of the communication graph. Furthermore, perception tasks, execution of the current action, and computation of the next action can all be performed asynchronously and concurrently. This has the potential to significantly improve the performance of the system, especially in multi-core processors.

The primary *contribution* of this paper is a learnable PAC framework composed of four asynchronous modules: perception, inter-robot communication, decentralized GNN message aggregation and inference, and low-level controller. The two key salient features of the framework are:
(1) Decentralized GNN: We leverage the aggregated GNN model [2] for decentralized message aggregation and inferencing. The model uses aggregated features comprising hidden outputs of the internal network layers. As the hidden layer outputs from neighboring robots are encoded in the messages, robots need not recompute graph convolutions performed by other robots, thereby distributing the computation over the robots. **(2) Asynchronous modules:** The framework is designed to execute perception and GNN computations asynchronously. This allows the message aggregation and inferencing to be performed at a much higher frequency than the computationally intensive perception tasks.

We also provide a ROS2 [13] compatible open-source implementation of the framework written primarily in C++ for PAC in robot swarms using GNNs.

II. Navigation Control Problem

The navigation control problem, in the paper, considers a homogeneous team of N mobile robots that needs to navigate through a d-dimensional environment $\mathcal{W} \subseteq \mathbb{R}^d$ to minimize the expected value of an application-defined cost function. We denote the set of robots by $\mathcal{V} = \{1, \ldots, N\}$, with the position of the i-th robot denoted by $\mathbf{p}_i(t) \in \mathcal{W}$ at time t. The state of

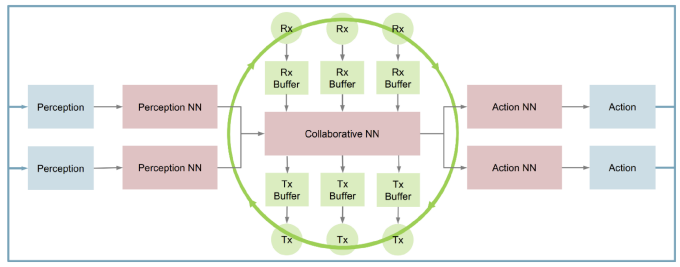

Fig. 2. Learning Perception-Action-Communication (PAC) loops using an architecture composed of three Neural Networks (NN): The perception NN, usually a Convolution NN, computes features using the sensor data obtained through perception. The core of the architecture is a collaborative NN, a Graph NN in our case, which computes the messages to be exchanged between robots and aggregates received messages. The GNN also computes features for the action NN, often a shallow Multi-Layer Perceptron (MLP), the output of which is sent to a planning and control module.

the i-th robot at time t is denoted by $\mathbf{x}_i(t) \in \mathbb{R}^m$, which, in addition to robot positions, may comprise velocities and other sensor measurements. The states of the multi-robot system and the control actions are collectively denoted by:

$$\mathbf{X}(t) = \begin{bmatrix} \mathbf{x}_1(t) \\ \mathbf{x}_2(t) \\ \vdots \\ \mathbf{x}_N(t) \end{bmatrix} \in \mathbb{R}^{N \times m}, \quad \mathbf{U}(t) = \begin{bmatrix} \mathbf{u}_1(t) \\ \mathbf{u}_2(t) \\ \vdots \\ \mathbf{u}_N(t) \end{bmatrix} \in \mathbb{R}^{N \times d}.$$

We consider the multi-robot system to evolve as per a Markov model $\mathbb{P}$, i.e., the state of the system at time $t + \Delta t$ depends only on the state of the system and the control actions at time t, where Δt is the time required for a single step.

$$\mathbf{X}(t + \Delta t) = \mathbb{P}(\mathbf{X} \mid \mathbf{X}(t), \mathbf{U}(t)) \tag{1}$$

The control problem can then be posed as an optimization problem, where the system incurs a cost given by a cost function $c(\mathbf{X}(t), \mathbf{U}(t))$ for state $\mathbf{X}(t)$ and control action $\mathbf{U}(t)$ taken at time t, and the goal is to find a policy Π_c^* that minimizes the expected cost [4]:

$$\Pi_c^* = \underset{\Pi_c}{\operatorname{argmin}}\, \mathbb{E}\left[\sum_{t=0}^{\infty} \gamma^t c(\mathbf{X}(t), \mathbf{U}(t))\right].$$

Here, the control actions are drawn from a conditional distribution $\mathbf{U}(t) = \Pi_c(\mathbf{U} \mid \mathbf{X}(t))$. Note that the policy Π_c^* is centralized as the control actions, in the above formulation, require complete knowledge of the state of the system.

A. Decentralized Navigation Control

In the decentralized navigation control problem, the robots take control actions based on their local information and the information communicated by their neighbors. Thus, we consider that the robots are equipped with a communication device for exchanging information with other robots that are within a given communication radius r_c. The problem can then be formulated on a *communication graph* $\mathcal{G} = (\mathcal{V}, \mathcal{E})$, where $\mathcal{V}$ represents the set of robots and $\mathcal{E}$ represents the

communication topology of the robots. A robot i can communicate with another robot j if and only if their relative distance is less than a given communication radius r_c, i.e., an edge $e = (i, j) \in \mathcal{E}$ exists if and only if $\|\mathbf{p}_i - \mathbf{p}_j\|_2 \leq r_c$. We assume bidirectional communication, and therefore, the communication graph is assumed to be undirected.

A robot i can communicate with its neighbors $\mathcal{N}(i)$, defined as $\mathcal{N}(i) = \{j \in \mathcal{V} \mid (j, i) \in \mathcal{E}\}$. Information can also be propagated through multi-hop communication. The set of k-hop neighbors that the robot i can communicate with at most k communication hops is defined recursively as:

$$\mathcal{N}_k(i) = \mathcal{N}_{k-1}(i) \cup \bigcup_{j \in \mathcal{N}_{k-1}(i)} \mathcal{N}(j), \quad \text{with } \mathcal{N}_0(i) = \{i\}.$$

Let $\frac{1}{\Delta t_c}$ be the frequency at which the robots communicate with each other, i.e., Δt_c is the time required for a single communication to take place. Then, the total information acquired by robot i is given by:

$$\mathcal{X}_i(t) = \bigcup_{k=0}^{\lfloor \frac{t}{\Delta t_c} \rfloor} \{\mathbf{x}_j(t - k\Delta t_c) \mid j \in \mathcal{N}_k(i)\}.$$

Now, the control actions can be defined in terms of a decentralized control policy π_i:

$$\mathbf{u}_i(t) = \pi_i(\mathbf{u}_i \mid \mathcal{X}_i(t)).$$

Denoting by $\mathbf{U}(t) = [\mathbf{u}_1(t), \ldots, \mathbf{u}_N(t)]^\top$ and $\mathcal{X}(t) = [\mathcal{X}_1(t), \ldots, \mathcal{X}_N(t)]^\top$, the decentralized control problem can be formulated as:

$$\Pi^* = \underset{\Pi}{\operatorname{argmin}}\, \mathbb{E}\left[\sum_{t=0}^{\infty} \gamma^t c(\mathcal{X}(t), \mathbf{U}(t))\right].$$

Computing the optimal decentralized policy is much more challenging than the centralized control as it contains the trajectory histories, unlike the Markov centralized controller [4]. The problem is computationally intractable for complex systems [14], which motivates the use of learning-based approaches. GNNs, in particular, are well-suited for decentralized control for multi-robot systems as they operate on the communication graph topology and can be used to learn a decentralized control policy from training data generated using a centralized controller.

Remark 1. Asynchronous Communication and Inference: The formulation for the centralized and decentralized control problems follows the structure given by Gama *et al.* [4]. However, similar to several other works on decentralized control, the formulation in [4] assumes that a single step of message aggregation and diffusion is performed at the same time step as the evolution of the system and perception tasks. In contrast, our formulation separates these tasks and executes them asynchronously at a higher frequency by explicitly parametrizing two different time steps. Asynchronous and decentralized execution of modules results in higher fidelity of the overall system.

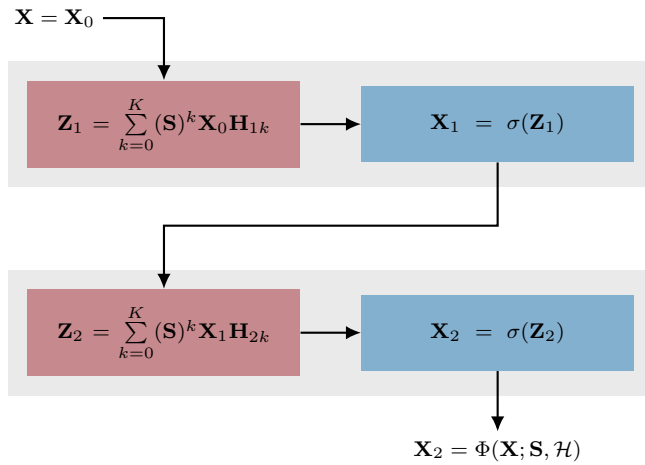

Fig. 3. A Graph Convolution Neural Network (GCNN) with two layers. Each layer is made up of a convolution graph filter followed by a point-wise non-linearity. GNNs are particularly suitable for decentralized robot swarms as the computations respect the locality of the communication graph.

III. Decentralized Graph Neural Networks

Graph Neural Networks (GNNs) [1] are layered information processing architecture that operate on a graph structure and make inferences by diffusing information through the graph. In the context of multi-robot systems, the graph is imposed by the communication graph, i.e., the graph nodes $\mathcal{V}$ represent the robots, and the edges represent the communication links $\mathcal{E}$, as discussed in Section II-A. In this paper, we focus on Graph Convolutional Neural Networks (GCNNs), a layered composition of convolution graph filters with point-wise non-linearities (σ). The architecture is defined by L layers, K hops of message diffusion, and a *graph shift operator* $\mathbf{S} \in \mathbb{R}^{N \times N}$, $N = |\mathcal{V}|$ that is a based on the communication graph. The elements $[\mathbf{S}]_{ij}$ can be non-zero only if $(i, j) \in \mathcal{E}$. The input to the GCNN is a collection of features $\mathbf{X}_0 \in \mathbb{R}^{N \times d_0}$, where each element $\mathbf{x}_i$ is a feature vector for robot i, $\forall i \in \mathcal{V}$. The weight parameters for learning on GNNs are given by $\mathbf{H}_{lk} \in \mathbb{R}^{d_{(l-1)} \times d_l}$, $\forall l \in \{1, \cdots, L\}$, $\forall k \in \{1, \cdots, K\}$, where d_l is the dimension of the hidden layer l with d_0 as the dimension of the input feature vectors. The convolution graph filters are polynomials of the graph shift operator $\mathbf{S}$ with coefficients defined by the input and the weight parameters $\mathbf{H}_{lk}$. The output $\mathbf{Z}_l$ of the filter is processed by a point-wise non-linearity σ to obtain the output of layer l, i.e., $\mathbf{X}_l = \sigma(\mathbf{Z}_l)$. The final output of the GCNN is given by $\mathbf{X}_L$, and the entire network is denoted by $\Phi(\mathbf{X}; \mathbf{S}, \mathcal{H})$. Figure 3 shows an architecture with two layers.

To see that GNNs are suitable for decentralized robot swarms, consider the computation $\mathbf{Y}_{kl} = (\mathbf{S})^k \mathbf{X}_{(l-1)}$ for some layer l. These computations can be done recursively: $\mathbf{Y}_{kl} = \mathbf{S}(\mathbf{S})^{(k-1)} \mathbf{X}_{(l-1)} = \mathbf{S}\mathbf{Y}_{(k-1)l}$. For a robot i, vector $(\mathbf{y}_i)_{kl} = [\mathbf{Y}_{kl}]_i$ can be computed as:

$$(\mathbf{y}_i)_{kl} = \sum_{j \in \mathcal{N}(i)} [\mathbf{S}]_{ij} (\mathbf{y}_j)_{(k-1)l} \tag{2}$$

Here, $\mathcal{N}(i)$ is the set of neighbors of robot i, and $[\mathbf{S}]_{ij}$ is the (i,j)-th element of the graph shift operator $\mathbf{S}$. Since the value of $[\mathbf{S}]_{ij}$ is non-zero only if $(i,j) \in \mathcal{E}$, the computation of $(\mathbf{y}_i)_{kl}$ only involves the features of the neighbors of robot i, i.e., the computation respects the locality of the communication graph. Thus, the robot i needs to only receive $(\mathbf{y}_j)_{(k-1)l}$ from its neighbors to compute $(\mathbf{y}_i)_{kl}$, which makes the overall system decentralized. The collection of hidden feature vectors $(\mathbf{y}_i)_{kl}$ forms the *aggregated message* [2] $\mathbf{Y}_i$ for robot i, which is precisely the information the robot i needs to communicate to its neighboring robots.

Definition 1. *Aggregated Message* $\mathbf{Y}_i$: The aggregated message for a robot i is defined as:

$$\mathbf{Y}_i = \begin{bmatrix} (\mathbf{y}_i)_{01} = (\mathbf{x}_i)_0 & (\mathbf{y}_i)_{11} & \cdots & (\mathbf{y}_i)_{(K-1)1} \\ \vdots & \vdots & \ddots & \vdots \\ (\mathbf{y}_i)_{0l} = (\mathbf{x}_i)_{l-1} & (\mathbf{y}_i)_{1l} & \cdots & (\mathbf{y}_i)_{(K-1)l} \\ \vdots & \vdots & \ddots & \vdots \\ (\mathbf{y}_i)_{0L} = (\mathbf{x}_i)_{L-1} & (\mathbf{y}_i)_{1L} & \cdots & (\mathbf{y}_i)_{(K-1)L} \end{bmatrix}$$

where, $(\mathbf{x}_i)_0$ is the input feature for robot i, $(\mathbf{x}_i)_l$ is the output of layer l of the GNN, and

$$(\mathbf{y}_i)_{kl} = \sum_{j \in \mathcal{N}(i)} [\mathbf{S}]_{ij} (\mathbf{y}_j)_{(k-1)l}, \quad \forall k \in \{1, \cdots, K-1\}, \forall l \in \{1, \cdots, L\} \tag{3}$$

Note that the dimension of each vector in a row is the same, but the dimension across rows may be different, i.e., $\mathbf{Y}_i$ is a collection of matrices and not a proper tensor.

The overall algorithm for message aggregation and inference using a GNN is given in Algorithm 1. The output of the GNN is the output of the last layer $\mathbf{X}_L$. To completely diffuse a signal $\mathbf{x}_i$ across the network, each robot needs to exchange messages and execute Algorithm 1 for KL times. This would require that the GNN message aggregation must be executed at a frequency that is KL times higher than the frequency of perception. Depending on the application and the number of layers of the network, this may not always be feasible. However, due to the stability properties of the GNNs, they perform well even when the message aggregation is executed at a lower frequency.

Remark 2. The computation of each individual element of $(\mathbf{y}_i)_{kl}$ is a single matrix multiplication, as the computation of $(\mathbf{y}_j)_{(k-1)l}$ is already performed by the neighboring robot j. Thus, aggregated GNNs naturally distribute computation across robots. Furthermore, the size of the aggregated message $\mathbf{Y}_i$ is defined by the architecture of the GNN, the dimension of the input feature vector, and the dimension of the output. It is independent of the number of robots in the system, making it scalable to large robot swarms. These properties make the aggregated GNNs suitable for decentralized robot swarms and, therefore, are used in the proposed framework for asynchronous PAC.

Algorithm 1: GNN Aggregation and Inference

Input : Messages $\{\mathbf{Y}_j \mid j \in \mathcal{N}(i)\}$, model parameters $\mathcal{H}$
Output : Inference output $(\mathbf{x}_i)_L$, messages $\mathbf{Y}_i$

$(\mathbf{x}_i)_0 \leftarrow \mathbf{x}_i$; `// Input feature for robot i`
for $l = 1$ **to** L **do**
  $(\mathbf{y}_i)_{0l} \leftarrow (\mathbf{x}_i)_{l-1}$;
  $\mathbf{z}_l \leftarrow (\mathbf{y}_i)_{0l} \mathbf{H}_{lk}$;
  for $k = 1$ **to** K **do**
    $(\mathbf{y}_i)_{kl} \leftarrow \mathbf{0}$;
    for $j \in \mathcal{N}(i)$ **do**
      $(\mathbf{y}_i)_{kl} \leftarrow (\mathbf{y}_i)_{kl} + [\mathbf{S}]_{ij} (\mathbf{y}_j)_{(k-1)l}$;
    end
    $\mathbf{z}_l \leftarrow \mathbf{z}_l + (\mathbf{y}_i)_{kl} \mathbf{H}_{lk}$;
  end
  $\mathbf{z}_l \leftarrow \mathbf{z}_l + \mathbf{b}_l$; `// If bias is used`
  $(\mathbf{x}_i)_l \leftarrow \sigma(\mathbf{z}_l)$; `// Point-wise non-linearity`
end
$\mathbf{Y}_i \leftarrow [\mathbf{x}_i, (\mathbf{y}_i)_{kl}]$; `// Def. 1`

IV. Asynchronous PAC Framework

The framework is designed to efficiently perform decentralized and asynchronous Perception-Action-Communication (PAC) loops in robot swarms. It comprises four primary modules for different PAC subtasks that are executed asynchronously: (1) Perception, (2) Inter-Robot communication, (3) GNN message aggregation and inference, and (4) Low-level actuator controller. The asynchronous design of the framework is motivated by two main advantages:

Concurrent execution: Asynchronous modules allow non-related subtasks to be executed concurrently, especially the computationally expensive perception module and relatively faster GNN module. As a result, the GNN module can perform several steps of message aggregation, thereby diffusing information over a larger number of nodes in the communication graph, while the perception module is still processing the sensor data. Furthermore, concurrent execution significantly reduces the computation time when executed on multi-core processors, thereby enabling better real-time performance.

Variable frequency: Asynchronous modules allow different subtasks to be executed at different frequencies. In particular, the GNN module can be executed at a lower frequency than the perception module, which has not been possible in prior work. Similarly, as is often the case, the communication and the low-level actuator controller modules can run at a higher frequency than the GNN message aggregation module. Generally, a GNN policy computes a high-level control action, which is then executed by a low-level controller for several time steps. Even in the case where the perception task is minimal, asynchronous execution allows the GNN module to perform several steps of message aggregation while the low-level controller is executing the previous control action.

In prior work, the perception and GNN computations were considered to be executed synchronously, even if communication and low-level controller are asynchronous, affecting the computation time and the number of message aggregations that can be performed by the GNN module. This is mitigated in

our proposed framework by allowing asynchronous execution.

The system is physically realized across three domains: the robot (Section IV-B and Section V), the Ground Control Station (GCS) (Section IV-E) and the Communication network (Section VI). These three domains are staffed by an ensemble of ROS2 nodes run inside Docker containers deployed on the robots and the ground control station (GCS), while the Communication network serves as the incorporeal substrate. The use of containers is crucial to the software maintenance and the bring-up of a fleet of robots. We now describe the different modules and components of the framework.

A. Coordinate Frames

It is instructive to cast the system's components in terms of their place in the set of four coordinate frames that are held in the system. These are: the *mission* frame $\mathcal{F}_M$, the North-East-Down (NED) *local* frame $\mathcal{F}_L$, the Front-Right-Down (FRD) *body* frame $\mathcal{F}_L$ and the *global* frame (Latitude and Longitude) $\mathcal{F}_G$. The complete set of frames is used on-board the vehicle and the ground control station deals only in coordinates referenced to $\mathcal{F}_M$ and $\mathcal{F}_G$. The key transform is between from $\mathcal{F}_M$ to $\mathcal{F}_L$, $\mathbf{T}_M^L$ and its inverse $\mathbf{T}_L^M = \mathbf{inv}(\mathbf{T}_M^L)$ because this is how positions and actions are transformed between LPAC to the flight controller and vice-versa; Figure 4.

B. LPAC

The LPAC node grants each robot autonomy and serves as the pilot; it operates exclusively in $\mathcal{F}_M$. It ingests sensory readings and positions as the robot traverses the IDF, as well as the perceptual embeddings $\mathbf{x}_j$ and positions ${}^M\mathbf{p}_j$ in the mission frame received from neighboring robots ($j \in \mathcal{N}(i)$). From this input, LPAC produces the velocity ${}^M\mathbf{v}_i$ that is delivered to the Offboard node to be transformed to ${}^L\mathbf{v}_i$.

In our implementation, we set the Perception module to refresh the embedding $\mathbf{x}_i$ at a rate of 5 Hz. We configure the GNN-based Communication module to query the message buffer manager, which holds positions and embeddings received from other robots $[\mathbf{x}_j, {}^M\mathbf{p}_j]$, at a rate of 2.5 Hz. Operating the Communications module at a lower frequency is a design decision that allows a greater window for aggregation. The robot's velocity is read from the output buffer of the Action module and sent to the low-level flight controller at a rate of 10 Hz.

1) Perception: The perception module is responsible for getting the sensor data and processing it to obtain the input features for the GNN. The module may also contain application-specific tasks such as semantic mapping, object detection, and localization, which makes the module computationally expensive. The entire perception module is typically executed at a low frequency in applications that require significant computation. In our specific implementation for the coverage control problem in Section VII, we use a CNN to generate a low-dimensional feature vector for the GNN module.

2) Inter-Robot Communication: Robots *broadcast* their message $\mathbf{Y}_i$, for robot i, to other robots within their communication range r_c, i.e., the neighboring robots $\mathcal{N}(i)$. They

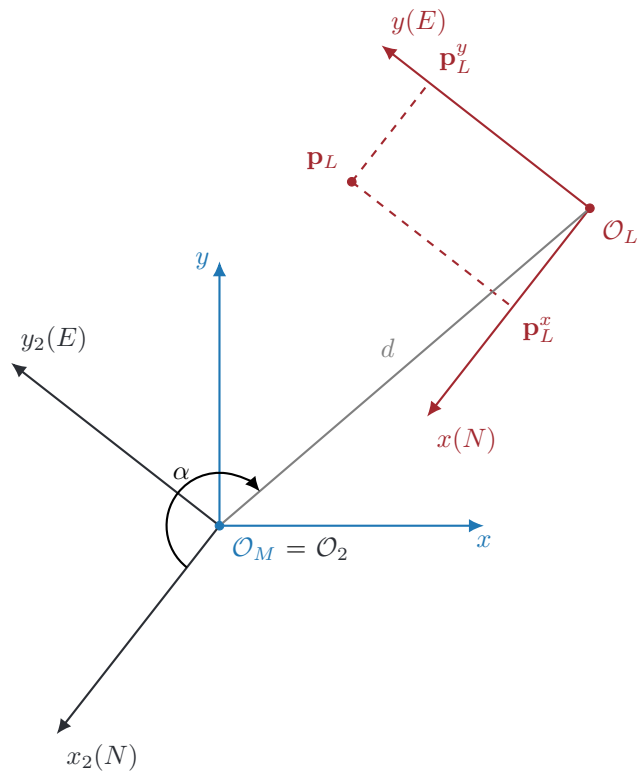

Fig. 4. Translation between $\mathcal{F}_M$ and $\mathcal{F}_L$ determined by the azimuth α and the distance d between the mission origin $\mathcal{O}_M$ to the local origin $\mathcal{O}_L$. The phasor $d\angle\alpha$ is computed using the GPS coordinates of the vehicle at boot and the mission origin sent to it by the GCS.

also receive messages from their neighbors: $\mathbf{Y}_j, \forall j \in \mathcal{N}(i)$. Generally, communication hardware may allow either receiving a message or transmitting a message at a given time. Thus, the communication module may need to be executed twice the frequency of the GNN message aggregation module. We use two buffers to maintain messages: a transmitter buffer $\mathrm{T_x}$, which stores the message to be transmitted, and a receiver buffer $\mathrm{R_x}$, which stores the most recent message received from each neighbor. The module is composed of three submodules: a message buffer manager, a transmitter, and a receiver.

Message Buffer Manager: The message buffer manager handles the transmitter $\mathrm{T_x}$ and receiver $\mathrm{R_x}$ buffers. When a new message is generated by the GNN module, the message buffer performs five sequential actions (1) momentarily locks the transmitter and receiver to avoid race conditions in writing and reading the buffers, (2) loads the new message $\mathbf{Y}_i$, received from the GNN module, onto the transmitter buffer, (3) sends the contents of the receiver buffer to the GNN module, (4) clears the receiver buffer, and (5) releases the lock on the buffers. Since having a lock on the communication buffers is not desirable, our implementation makes efficient use of *smart*

memory pointers in C++ to exchange the contents from the GNN module and the buffers, i.e., the actual contents are not loaded to the buffers, but the pointers to the memory locations are exchanged. Clearing the receiver buffer is critical to ensure old messages, which would have been used in the previous GNN message aggregation, are not considered further.

Transmitter: The transmitter submodule broadcasts the message $\mathbf{Y}_i$, using the $\mathrm{T_x}$ message buffer, to neighboring robots $\mathcal{N}(i)$. Additionally, an identification is attached to the message so that the receiving robot can rewrite old messages in the buffer with the most recent message from the same robot.

Receiver: The receiver submodule receives the messages broadcast by the neighboring robots $\mathcal{N}(i)$. If a message is received from a robot that already has a message in the receiver buffer, the message is overwritten with the most recent message, i.e., only the most recent message from a neighboring robot is stored in the receiver buffer. The size of the buffer needs to be dynamic as it is dependent on the number of neighbors, which may change over time.

3) GNN Message Aggregation and Inference: The GNN message aggregation module has two tasks: (1) generate messages to be communicated to neighboring robots in the next time step, and (2) perform inference for control actions. Our framework uses the aggregated GNN model, described in Section III. The system is fully decentralized, i.e., each robot has its own GNN model, and the inference is performed locally. An important attribute of the aggregated GNN model is that the size of the messages is dependent on the number of layers in the network, and is independent of the number of robots. Thus, the system is highly scalable to large robot swarms. The module is executed at a higher frequency than the perception module.

C. Offboard.

The offboard node manages the frame transformations between $\mathcal{F}_M$ and $\mathcal{F}_L$, and the state machine that, in turn, governs the mode of the robot. The frame transformations $\mathbf{T}_M^L$ and $\mathbf{T}_L^M$ require the computation of the phasor $d\angle\alpha$ with translation d and azimuth α, which can be found using a geodesic inverse function [15]. We can therefore define the translation for $\mathbf{T}_L^M$, $\mathbf{t}_L^M = [d_x, d_y, d_z] = d[\cos(\alpha), \sin(\alpha), 0]$, where we assume that there is no difference in altitude between the frames. Using $\mathbf{t}_L^M$ and the heading θ which captures the difference in frame orientation between $\mathcal{F}_L$ and $\mathcal{F}_B$ we can express the transform in terms of its rotational and translational parts,

$$\mathbf{T}_L^M = \left[\begin{array}{c|c} \mathbf{R}_z\mathbf{R}_x & \mathbf{t}_L^M \\ \hline 0 & 1 \end{array}\right] \quad \text{where,} \tag{4}$$

$$\begin{aligned} \mathbf{R}_z &= \begin{bmatrix} \cos\left(\frac{3\pi}{2}-\theta\right) & -\sin\left(\frac{3\pi}{2}-\theta\right) & 0 \\ \sin\left(\frac{3\pi}{2}-\theta\right) & \cos\left(\frac{3\pi}{2}-\theta\right) & 0 \\ 0 & 0 & 1 \end{bmatrix}, \\ \mathbf{R}_x &= \begin{bmatrix} 1 & 0 & 0 \\ 0 & \cos\pi & -\sin\pi \\ 0 & \sin\pi & \cos\pi \end{bmatrix} \end{aligned} \tag{5}$$

.

We compose the rotation $\mathbf{R}_z\mathbf{R}_x$ because the mission frame is established by pointing the robot's body frame x-axis in the direction of the mission frame's y-axis and record the heading θ (a convention chosen because it is easier to teleoperate a robot when it faces away from the operator). Therefore, we are first obliged to rotate a point in $\mathcal{F}_L$ about the x-axis by $180°$ followed by a rotation about the z-axis where the offset $3\pi/2$ comes from the fact that we originally defined θ to be the angle between $\mathcal{F}_M^{(y)}$ and $\mathcal{F}_L^{(x)}$.

The LPAC system is designed to maneuver vehicles on a 2D plane. Behavior along the vertical z-axis is completely independent of the LPAC control policy. Therefore, the Offboard node uses a simple proportional controller to drive each robot to a fixed altitude:

$$v_z = -K_p(\mathbf{p}_z^{(d)} - \mathbf{p}_c^{(c)}) \tag{6}$$

Where $\mathbf{p}_z^{(d)}$ and $\mathbf{p}_z^{(c)}$ denote the desired position and current position along the vertical axis, respectively. We found that setting the proportional gain to $K_p = 1$ worked well in practice.

The offboard node maintains the operational state-machine of the robot throughout an experiment. The machine receives messages from the GCS mission control node as the control input to progress the robot through a deployment. The offboard node controls all actuation while the robot is not in the Mission state. After takeoff altitude is reached, the offboard node begins transforming the velocities ${}^M\mathbf{v}_i$ from the LPAC node to the low-level flight controller.

D. Low-Level Controller

The low-level controller interfaces the framework with the robot actuators. It receives the control action at the end of the computation of the GNN module and executes it for a pre-defined time interval. The controller is executed at a very high frequency to ensure that the control actions are reliably executed in real time while correcting the control commands using a feedback loop. We use the PX4 flight controller which is an off-the-shelf autopilot software stack that abstracts the low-level actuation of the robot. It tracks both the local and global frames of the vehicle and therefore operates in $\mathcal{F}_L$ and $\mathcal{F}_G$. The PX4 interface is exposed to ROS2 through a MicroDDS pipeline [16] which enables reading the positions in the aformentioned frames and sending velocity commands to the robot. The origin $\mathcal{O}_L$ of $\mathcal{F}_L$ is determined at vehicle boot and the position in the frame is estimated using an Extended Kalman Filter (EKF) to fuse sensor readings. LPAC produces velocities ${}^M\mathbf{v}_i$ in $\mathcal{F}_M$ which are transformed to the local frame, ${}^L\mathbf{v}_i = \mathbf{T}_M^L\,{}^M\mathbf{v}_i$. Likewise, positions from the flight controller ${}^L\mathbf{p}_i$ can be transformed to the mission frame, ${}^M\mathbf{p}_i = \mathbf{T}_L^M\,{}^L\mathbf{p}_i$ to be used by LPAC. Since the implementation of the framework is designed to work with ROS2, any existing package for low-level control can be used with the framework.

Fig. 5. We use the ModalAI Starling 2 as our robot platform. The vehicle has onboard compute running both the flight controller and LPAC. Localization is accomplished using GNSS as well as inertial and barometric measurements. Inter-vehicle communication is handled by the onboard WiFi radios.

E. Ground Control Station

1) Mission Control. : The Mission Control node is run on the GCS laptop and is the operator's access panel to the state machine run in the offboard node on-board each robot. It includes safety features such as a geofence and the ability to severe autonomy and force the robots to hold position at the flip of a virtual switch. A routine experiment would involve the operator enabling the system, initiating takeoff, observing the mission and finally initiating a landing. The Mission Control node communicates with all robots on the network using a mission control ROS2 topic. The node also includes a field for specifying $\mathcal{O}_M$ in terms of the Latitude, Longitude and heading, which is then distributed to all robots on the network.

2) Mission Visualization. : A live view of the robots progress on coverage control is visualized by instantiating a local Coverage Control Simulator node on the GCS which receives positions from the robots. We remark that the simulator on the GCS does not influence the behaviour of the robots and is entirely for visualization purposes. The view of the agents overlaying the density function is rendered in RViz.

V. Autonomous Aerial Vehicle Hardware

A. Airframe and Compute

Autonomous aerial vehicles (AAV) serve as the main robotics platform for demonstrating the efficacy and robustness of our system. We use 10 of ModalAI's Starling 2 quadrotor robots in each of our experiments. Our chosen platform is size weight and power (SWaP) limited; the $220\,\mathrm{mm}$ airframe weighs only $280\,\mathrm{g}$ [17]. From the factory, each Starling 2 is equipped with a Qualcomm QRB5165 processor mounted on a VOXL2 single board computer (SBC). The 64 bit ARM processor has 8 cores that are able to reach clock speeds of 2.84 GHz and is supported by 8GB of LPDDR5 memory [18]. LPAC inference and PX4 v1.14 autopilot run in tandem on the same on-board VOXL2 computer. The VOXL2 runs a modified version of Ubuntu 18.04 with the 4.19.125 kernel.

B. Sensors

The focus of our experiments is on LPAC as a control policy and the interaction between agents via embeddings shared over the network. We operate under the assumption that the map of the environment has already been generated. Each robot must be able to localize itself in our mission frame $\mathcal{F}_M$ and maintain a fixed altitude. The simulated sensor coverage provided by each robot is constant and independent of altitude. Out of the box, the autopilot runs an extended Kalman filter (EKF) for sensor fusion. The vehicle is equipped with the uBlox-M10S GNSS receiver, QMC5883L compass, two TDK ICM-42688-P inertial measurement units (IMU) and two barometers: a Bosch BMP388 and a TDK ICP-10100. We configure the EKF to fuse GNSS, IMU and barometer measurements for localization. The Starling 2 includes several cameras, which we disable to save resources.

C. Communication

LPAC relies on communication between agents. Each robot agent has an ALFA AWUS036EACS WiFi radio operating in the $5\,\mathrm{GHz}$ band. The radio has a typical power output of 17 dBm and has an integrated antenna. A single TP-Link AX1800 WiFi router manages traffic from vehicle to vehicle and between each vehicle and the ground control station (GCS). All radios in the system support the 802.11ac WiFi standard, enabling a maximum data-rate of 433 Mbps.

VI. Network Configuration and Performance

The agents communicate over an 802.11-based wireless network operating in infrastructure mode with a shared access point (AP). To maximize coverage, the WiFi AP is centrally placed within the environment. For larger testing areas, configurations involving multiple routers connected via Ethernet have also been considered. This centralized setup simplifies coordination, as a single node manages all communication. However, such architectures can suffer from single points of failure and limited scalability as the number of agents grows. These trade-offs appear in any policy that involves inter-agent communication. Nonetheless, our architecture is agnostic to the structure of the communications network due to the inherent flexibility of the GNN. We use a centralized setup for the communications while computations remain decentralized. To support more scalable and fault-tolerant deployments, we have

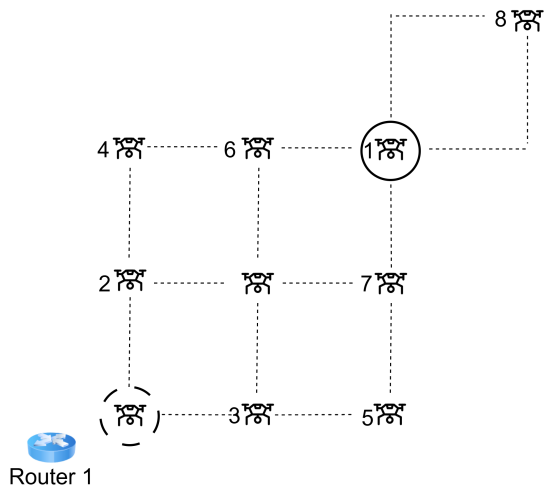

Fig. 6. Configuration for the throughput tests. An iPerf3 server was initialized in the drone with a dashed circle, while the drone with a continuous circle was configured as a client. Initially, only the first three robots in the diagonal were turned on. The other agents were turned on progressively.

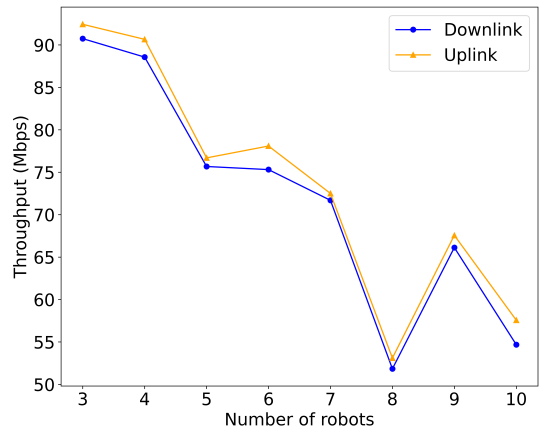

Fig. 7. Evolution of throughput measured in the network as the number of robots increases.

	Uplink throughput (Mbps)	**Downlink throughput (Mbps)**
Without Zenoh	43.16 ± 7.56	42.66 ± 7.58
With Zenoh	83.30 ± 1.45	82.89 ± 1.43

TABLE I
THROUGHPUT ACHIEVED FOR A CONFIGURATION WITH AND WITHOUT THE ZENOH PROTOCOL.

identified Doodle Labs radios [19] as a promising alternative for enabling fully distributed communication. Initial testing with these radios has yielded promising results, and they will be used in future implementations.

To better assess the quality of the network, we measured throughput using iPerf3 over a 10-second interval, varying the number of connected robots. The test configuration is shown in Figure 6, with the robots inside a dashed and continuous circle representing the iPerf3 server and client, respectively. Throughput was selected as the evaluation metric because it reflects overall network performance, capturing the effects of latency, jitter, and packet loss. The LPAC setup was disabled during these experiments to better evaluate the intrinsic network quality. For worst-case analysis, we focused on a drone located far from the router, and only considered one quadrant of the router's coverage—assuming that only neighboring agents in that sector are relevant for the selected agent. As shown in Figure 7, network performance degrades as the number of connected robots increases. The bandwidth limitations of centralized network topologies highlight that a decentralized network is more amenable to teams with more than 10 agents.

In initial experiments with 10 agents, we observed significant packet loss and latency, which hindered the smooth execution of the system. These issues highlighted the limitations of the default ROS2 middleware, DDS. Recent studies suggest that replacing DDS with the Zenoh protocol can improve both network performance and CPU utilization in wireless settings [20], [21]. To assess the potential benefits of this switch, we conducted a throughput test using the first three agents positioned along the diagonal in Figure 6. Each test ran for 60 seconds and was repeated 10 times under two configurations: using the default DDS and using Zenoh. To simulate network stress, the Docker containers on the robots were remotely restarted from the ground control station (GCS) during each interval. The average throughput across the 10 repetitions is reported in Table I. The results show that throughput is significantly higher when the Zenoh middleware is used. This enables more efficient data transmission by filtering and aggregating lower-level messages. Zenoh integrates seamlessly with ROS2, acting as a lightweight and high-performance alternative to the default DDS middleware. It enables communication across ROS2 nodes by bridging publish/subscribe and query/update paradigms in a unified protocol. This architecture reduces bandwidth usage and latency, making it especially suitable for dynamic and resource-constrained environments.

VII. REAL-WORLD COVERAGE EXPERIMENTS

Coverage control requires the collaboration of a robot swarm to provide sensor coverage to monitor a phenomenon or features of interest in an environment. An *importance density function* (IDF) [5] is used to model the probability distribution of features of interest. The problem is widely studied in robotics and has applications in various domains, including mobile networking [22], surveillance [23], and target tracking [24]. We consider the asynchronous setup where the robots have limited sensing capabilities. Furthermore, the environment is not known a priori, and the robots use their sensor to make localized observations of the environment.

Coverage control is posed as an optimization problem using *Voronoi partitions* $\mathcal{P}_i$ to assign each robot a distinct subregion of the environment [25], [26], [5]. The objective of the coverage problem is to minimize the cost to cover the

environment, weighted by the IDF $\Phi(\cdot)$, see [26] for details.

$$\mathcal{J}(\mathbf{p}_1, \ldots, \mathbf{p}_{|\mathcal{V}|}) = \sum_{i=1}^{|\mathcal{V}|} \int_{\mathcal{P}_i} \|\mathbf{p}_i - \mathbf{q}\|^2 \Phi(\mathbf{q}) \mathbf{d}\mathbf{q} \tag{7}$$

We model a $1024\,\mathrm{m} \times 1024\,\mathrm{m}$ rectangular environment and robots that make $64\,\mathrm{m} \times 64\,\mathrm{m}$ localized sensor observations. Each robot maintains a local map of size $256\,\mathrm{m} \times 256\,\mathrm{m}$ with cumulatively added observations and an obstacle map of the same size for the boundaries of the environment. Based on our contemporary work on coverage control, these maps are processed by a CNN with three layers of 32 latent sizes each. Additionally, relative positions of neighboring robots, obtained either through sensing or communication, within a communication radius of $128\,\mathrm{m}$ is mapped onto a two-channel (x and y) normalized heatmap. These four maps are concatenated to form the input to a CNN, which is composed of three layers of 32 latent sizes and generates a 32-dimensional feature vector for each robot. The sensing and processing of maps by CNN constitute the perception module of the PAC framework. The output of the CNN is augmented with the normalized position of the robot to form a 34-dimensional feature vector, which is used as the input to the GNN with two layers of 256 latent size and $K = 3$ hops of communication. The output of the GNN is processed by a multi-layer perceptron (MLP), i.e., an action NN, with one hidden layer and 32 latent sizes to compute the control velocities for the robot. These CNN and GNN architectures originate from [27].

The entire model is trained using imitation learning with the ground truth generated using a centralized clairvoyant Lloyd's algorithm that has complete knowledge of the IDF and the positions of the robots. We evaluate our approach for asynchronous Perception-Action-Communication (PAC) on the coverage control problem [28] for a swarm of 10 robots in the real world. Our experiments are conducted outdoors with a team of 10 autonomous aerial vehicles (robot). The terrain is grassy, flat and contains no obstacles within the defined mission boundaries. Ten elevated launch pads are distributed uniformly throughout the environment. Each robot is assigned to a launch pad which is maintained throughout the experiments. We did this to this ensure consistency between experiments, as each robot has slight hardware peculiarities that make it unique. During our experiments, there were some instances of robot failure. In this case, we substituted an identical robot from our reserve to complete the remaining experiments.

Evaluation in the real-world was carried out in two experiments (E1) Transferability and (E2) Repeatability. (E1) tests the system's performance under three different randomly generated IDFs; each with 10 Gaussian features. The purpose of (E2) is to assess the system's behavior when subjected to the high variance of the real world. Localization, relying primarily on GPS, is especially susceptible to noise. The localization error can vary between robots as a result of variances in hardware and their location. For example, some robots have stronger GPS reception than others. Often, robots must operate with horizontal positional error in the range of $1 - 5\,\mathrm{m}$. For (E3), during each experiment, we intentionally perturb the system by taking manual control of one robot. The robot is removed from the mission area, before it is manually returned. We only initiate perturbation once the system appears to have reached steady state. We always perturb the same drone and return it to approximately the same location near the mission boundary.

The original LPAC model was trained on an environment size of 1024×1024 with N robots and F Gaussian features where $N = F = 32$. There, the density of robots was $3.1e - 5$ robots/cell. For our experiments we selected a similar density of $3.8e - 4$ robots/cell by reducing the environment size to 512×512 and using $N = F = 10$. We maintain this environment size and density for all experiments. Deploying the system on an environment of size $512 \times 512\,\mathrm{m}^2$ is impractical for iterative development and experimentation. Robot positions are scaled by a factor of $16\ \mathrm{m}^{-1}$ to obtain a practical mission area of $32 \times 32\,\mathrm{m}^2$. The scale factor is applied between the LPAC model and the offboard controller. This enables us to operate LPAC closer to the environment size used during training while deploying in a confined area.

The maximum output speed of the model is $5\,\mathrm{m\,s}^{-1}$. To deploy in a smaller environment, we reduce the velocity using a scale factor of 0.25, resulting in a maximum speed of $1.25\,\mathrm{m\,s}^{-1}$.

A. Transferability

A key boon of LPAC is its transferability to new environments. We verify that this property still holds in the real world by deploying our system in three unknown environments outside of the training set. The start locations for each robot are the same across all three environments.

Snapshots from these experiments are shown in Figure 8. In all three environments, the LPAC policy achieves coverage of the importance field. The global map is overlayed with low opacity over each image of the map. This is purely for visualization and to demonstrate the efficacy of LPAC. The robots do not have access to any information outside of their local observations and embeddings from neighbors.

B. Repeatability

Under ideal, noiseless conditions, LPAC is a deterministic control policy. The real-world contains noise. We study its effect on LPAC by running the same experiment three times and observing the behavior of the system. Each experiment is run with robots starting from the same launch positions (a placement error within $10\,\mathrm{cm}$). The cost over time is plotted in Figure 9. The three cost traces capture the normalized coverage cost of each experiment within a window of $40\,\mathrm{s}$ from takeoff. This allows the system to converge to a stable coverage cost. The final cost achieved in all three experiments is similar despite differences in convergence rate. Despite physically placing the robots on the same launch pads, the localization error is significant. This error is magnified when the robots are

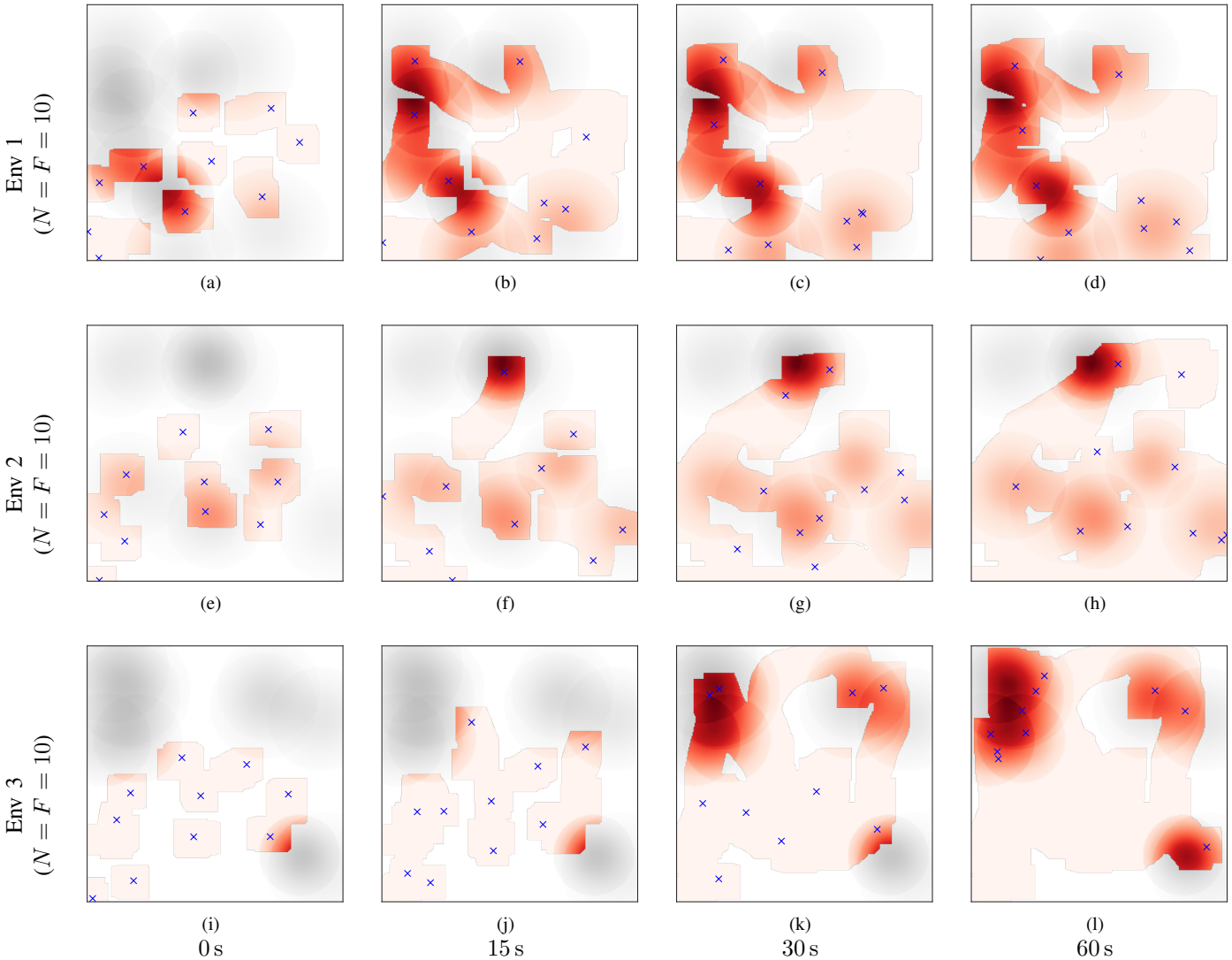

Fig. 8. Performance of the LPAC system in the real world across three different environments in a $32 \times 32\,\mathrm{m}^2$ area. Each environment contains $N = F = 10$ robots and Gaussian features. Convergence typically occurs within $60\,\mathrm{s}$ and is dependent on environment and initial positions of the robots. The $\times$ markers denote the positions of the robots in the environment, while the IDF is illustrated in red. Each robot has a $4 \times 4\,\mathrm{m}^2$ sensor area with which it explores the environment. The environment outside this sensor area is initially unknown to the agents, colored white here. We include a low opacity grayscale rendering of the IDF in unexplored regions to better convey coverage.

near the ground and GNSS suffers from signal blockage and multipath interference. We capture the differences in initial and final positions between each of the three trials in Figure 10.

VIII. Conclusion

We presented a framework for asynchronous Perception-Action-Communication with Graph Neural Networks (GNNs). Perception comprises application-specific tasks such as sensing and mapping, while the action module is responsible for executing controls on the robot. The GNN bridges these two modules and provides learned messages for collaboration with other agents. The decentralized nature of the GNN enables scaling to large robot swarms. The asynchronous capability of our system allows the execution of GNN-based message aggregation and inferencing at a frequency in between that of perception and action modules. We demonstrated the effectiveness of using learnable PAC policies in a decentralized manner for real-world incarnations of the coverage control problem. The framework is scalable and allows the evaluation and deployment of asynchronous PAC systems with GNNs with large robot swarms.

Future work entails validating the system with even larger scale teams and decentralized communications. We also plan to evaluate our framework on other applications, such as flocking and target tracking, and analyze the compatibility of our framework with other GNN architectures.

References

[1] T. N. Kipf and M. Welling, "Semi-Supervised Classification with Graph Convolutional Networks," in *International Conference on Learning*

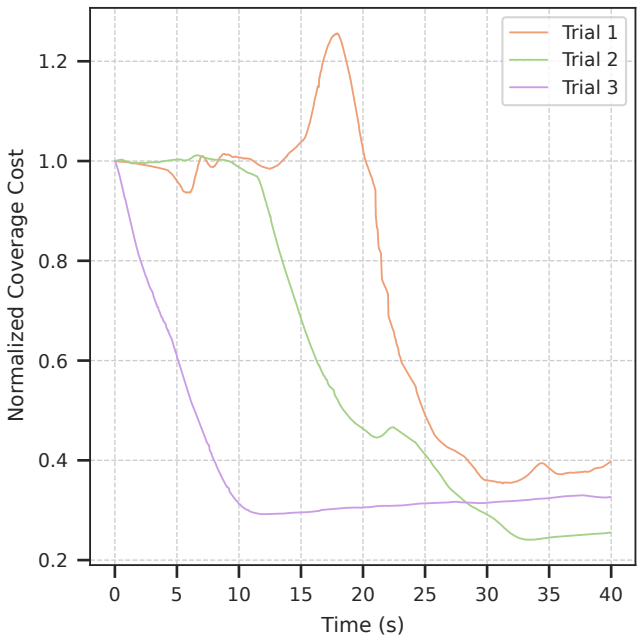

Fig. 9. Evaluating repeatability. The normalized coverage cost of three trials captured over 40 seconds. The beginning of each experiment occurs when the takeoff command is received. The trajectory of the cost varies between experiments but all ultimately reach a similar coverage cost. Factors such as noisy localization and wind play a significant role in how the quickly the robots converge to a solution in each trial.

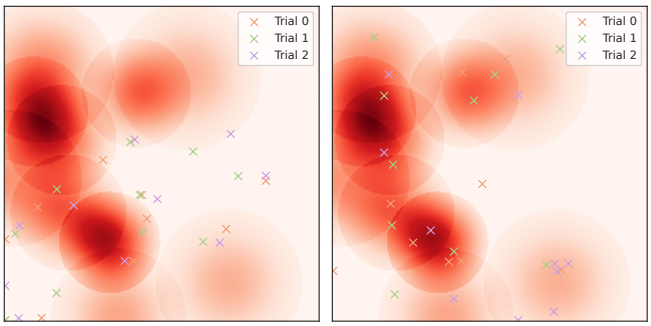

(a) $t = 0\,\mathrm{s}$ (b) $t = 40\,\mathrm{s}$

Fig. 10. Despite physically launching from the same site in each trial, the localization error in the robots is significant (left). The final reported local positions after 40 s (right) demonstrates the spread of positions once in the final timestep. A global view of the IDF is shown.

Representations, 2017.

[2] E. Tolstaya, F. Gama, J. Paulos, G. Pappas, V. Kumar, and A. Ribeiro, "Learning decentralized controllers for robot swarms with graph neural networks," in *Proceedings of the Conference on Robot Learning*, ser. Proceedings of Machine Learning Research, L. P. Kaelbling, D. Kragic, and K. Sugiura, Eds., vol. 100. PMLR, Oct 2020, pp. 671–682.

[3] E. Tolstaya, J. Paulos, V. Kumar, and A. Ribeiro, "Multi-robot coverage and exploration using spatial graph neural networks," in *2021 IEEE/RSJ International Conference on Intelligent Robots and Systems (IROS)*, 2021, pp. 8944–8950.

[4] F. Gama, Q. Li, E. Tolstaya, A. Prorok, and A. Ribeiro, "Synthesizing decentralized controllers with graph neural networks and imitation learning," *IEEE Transactions on Signal Processing*, vol. 70, pp. 1932–1946, 2022.

[5] W. Gosrich, S. Mayya, R. Li, J. Paulos, M. Yim, A. Ribeiro, and V. Kumar, "Coverage Control in Multi-Robot Systems via Graph Neural Networks," in *International Conference on Robotics and Automation (ICRA)*, 2022, pp. 8787–8793.

[6] Q. Li, F. Gama, A. Ribeiro, and A. Prorok, "Graph neural networks for decentralized multi-robot path planning," in *IEEE/RSJ International Conference on Intelligent Robots and Systems (IROS)*, 2020, pp. 11 785–11 792.

[7] L. Zhou, V. D. Sharma, Q. Li, A. Prorok, A. Ribeiro, P. Tokekar, and V. Kumar, "Graph neural networks for decentralized multi-robot target tracking," in *IEEE International Symposium on Safety, Security, and Rescue Robotics (SSRR)*, 2022, pp. 195–202.

[8] L. Ruiz, F. Gama, and A. Ribeiro, "Graph neural networks: Architectures, stability, and transferability," *Proceedings of the IEEE*, vol. 109, no. 5, pp. 660–682, 2021.

[9] W. L. Hamilton, R. Ying, and J. Leskovec, "Inductive representation learning on large graphs," in *Proceedings of the 31st International Conference on Neural Information Processing Systems*. Red Hook, NY, USA: Curran Associates Inc., 2017, p. 1025–1035.

[10] D. Owerko, F. Gama, and A. Ribeiro, "Predicting power outages using graph neural networks," in *IEEE global conference on signal and information processing*. IEEE, 2018, pp. 743–747.

[11] M. Tzes, N. Bousias, E. Chatzipantazis, and G. J. Pappas, "Graph neural networks for multi-robot active information acquisition," in *IEEE International Conference on Robotics and Automation (ICRA)*. IEEE, 2023, pp. 3497–3503.

[12] J. Blumenkamp, S. Morad, J. Gielis, Q. Li, and A. Prorok, "A framework for real-world multi-robot systems running decentralized gnn-based policies," in *International Conference on Robotics and Automation (ICRA)*, 2022, pp. 8772–8778.

[13] S. Macenski, T. Foote, B. Gerkey, C. Lalancette, and W. Woodall, "Robot operating system 2: Design, architecture, and uses in the wild," *Science Robotics*, vol. 7, no. 66, p. eabm6074, 2022.

[14] H. S. Witsenhausen, "A counterexample in stochastic optimum control," *SIAM Journal on Control*, vol. 6, no. 1, pp. 131–147, 1968.

[15] C. F. F. Karney, "Algorithms for geodesics," *Journal of Geodesy*, vol. 87, no. 1, p. 43–55, Jun. 2012. [Online]. Available: http://dx.doi.org/10.1007/s00190-012-0578-z

[16] eProsima, "Micro xrce-dds: Client/agent implementation of the dds-xrce protocol," https://micro-xrce-dds.docs.eprosima.com/, 2025, documentation v3.0.1; accessed 2025-09-21.

[17] ModalAI, Inc., "Voxl 2," https://www.modalai.com/products/voxl-2?variant=39914779836467, product page; Accessed 2025-09-21.

[18] Qualcomm Technologies, Inc., "Qualcomm dragonwing™ qrb5165 — robotics cpu with ai & 5g," https://www.qualcomm.com/products/internet-of-things/robotics-processors/qrb5165, accessed 2025-09-21.

[19] Doodle Labs - About Us. [Online]. Available: https://doodlelabs.com/about-us/

[20] J. Zhang, X. Yu, S. Ha, J. Peña Queralta, and T. Westerlund, "Comparison of middlewares in edge-to-edge and edge-to-cloud communication for distributed ros 2 systems," *Journal of Intelligent & Robotic Systems*, vol. 110, no. 4, Nov. 2024. [Online]. Available: http://dx.doi.org/10.1007/s10846-024-02187-z

[21] A. Corsaro, L. Cominardi, O. Hecart, G. Baldoni, J. E. P. Avital, J. Loudet, C. Guimares, M. Ilyin, and D. Bannov, "Zenoh: Unifying communication, storage and computation from the cloud to the microcontroller," in *2023 26th Euromicro Conference on Digital System Design (DSD)*, 2023, pp. 422–428.

[22] B. Hexsel, N. Chakraborty, and K. Sycara, "Coverage control for mobile anisotropic sensor networks," in *IEEE International Conference on Robotics and Automation*, 2011, pp. 2878–2885.

[23] L. Doitsidis, S. Weiss, A. Renzaglia, M. W. Achtelik, E. Kosmatopoulos, R. Siegwart, and D. Scaramuzza, "Optimal surveillance coverage for teams of micro aerial vehicles in gps-denied environments using onboard vision," *Autonomous Robots*, vol. 33, pp. 173–188, 2012.

[24] L. C. Pimenta, M. Schwager, Q. Lindsey, V. Kumar, D. Rus, R. C. Mesquita, and G. A. Pereira, "Simultaneous coverage and tracking (scat) of moving targets with robot networks," in *Algorithmic Foundation of Robotics VIII: Selected Contributions of the Eight International Workshop on the Algorithmic Foundations of Robotics*. Springer, 2010, pp. 85–99.

[25] Q. Du, V. Faber, and M. Gunzburger, "Centroidal Voronoi Tessellations: Applications and Algorithms," *SIAM Review*, vol. 41, no. 4, pp. 637–676, 1999.

[26] Cortés, Jorge, Martínez, Sonia, and Bullo, Francesco, "Spatially-distributed coverage optimization and control with limited-range interactions," *ESAIM: COCV*, vol. 11, no. 4, pp. 691–719, 2005.

[27] S. Agarwal, R. Muthukrishnan, W. Gosrich, V. Kumar, and A. Ribeiro, "Lpac: Learnable perception-action-communication loops with applications to coverage control," *CoRR*, vol. abs/2401.04855, 2024. [Online]. Available: https://doi.org/10.48550/arXiv.2401.04855

[28] B. Wang, "Coverage problems in sensor networks: A survey," *ACM Comput. Surv.*, vol. 43, no. 4, oct 2011.